

Semiclassical analysis of distinct square partitions

M. V. N. Murthy,¹ Matthias Brack*,² Rajat K. Bhaduri,³ and Johann Bartel⁴

¹*Institute of Mathematical Sciences, Chennai, 600 113 India*

²*Institute for Theoretical Physics, University of Regensburg, D-93040 Regensburg, Germany*

³*Department of Physics and Astronomy,*

McMaster University, Hamilton, Canada L9H 6T6

⁴*IPHC, Physique Théorique, Université de Strasbourg, F-67037 Strasbourg, France*

(Dated: August 16, 2024)

Abstract

We study the number $P(n)$ of partitions of an integer n into sums of distinct squares and derive an integral representation of the function $P(n)$. Using semiclassical and quantum statistical methods, we determine its asymptotic average part $P_{as}(n)$, deriving higher-order contributions to the known leading-order expression [M. Tran *et al.*, Ann. Phys. (N.Y.) **311**, 204 (2004)], which yield a faster convergence to the average values of the exact $P(n)$. From the Fourier spectrum of $P(n)$ we obtain hints that integer-valued frequencies belonging to the smallest Pythagorean triples (m, p, q) of integers with $m^2 + p^2 = q^2$ play an important role in the oscillations of $P(n)$. Finally we analyze the oscillating part $\delta P(n) = P(n) - P_{as}(n)$ in the spirit of semiclassical periodic orbit theory [M. Brack and R. K. Bhaduri: *Semiclassical Physics* (Bolder, Westview Press, 2003)]. A semiclassical trace formula is derived which accurately reproduces the exact $\delta P(n)$ for $n \gtrsim 500$ using 10 pairs of ‘orbits’. For $n \gtrsim 4000$ only two pairs of orbits with the frequencies 4 and 5 – belonging to the lowest Pythagorean triple (3,4,5) – are relevant and create the prominent beating pattern in the oscillations. For $n \gtrsim 100,000$ the beat fades away and the oscillations are given by just one pair of orbits with frequency 4.

* e-mail address: matthias.brack@ur.de

I. INTRODUCTION

Consider a one-dimensional trap with an integer-valued quantum spectrum. The problem of counting the number of excited states at a given energy E is the same as writing an integer as a sum of its parts. For example, partitioning the excitation energy in a harmonic spectrum is the same as partitioning an integer into a sum of other integers. Similarly, partitioning the excitation energy in a one-dimensional box with infinitely steep reflecting walls corresponds to partitioning an integer into sums of squares of integers [1]. This connection leads to a link between number theory and statistical mechanics. A partition may be fully unrestricted, allowing all possible sums with repetitions (bosonic), or allowing only distinct entries in the summands (fermionic). It may also be restricted by allowing only a fixed number N of summands in each partition.

Asymptotic formulae for large n are known following the work of Hardy and Ramanujan [2] and are found in many text books (see, e.g., [3]). This year marks the centenary of the publication of the famous paper by Hardy and Ramanujan [2], and it is appropriate to study the problem further. In particular, it is worthwhile to examine the number $P(n)$ of partitions of an integer n into sums of distinct squares (hereafter called F2 partitions), which contain some unique features. As was pointed out in Ref. [1], the exact function $P(n)$ for distinct square partitions exhibits pronounced oscillations with a beat-like structure when the points are joined by a continuous curve, as shown in Fig. 1 (cf. also Figs. 2 and 3 below).

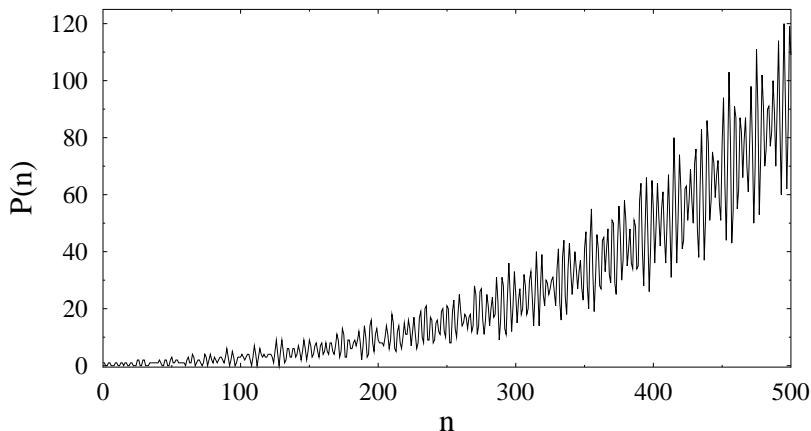


FIG. 1: $P(n)$ of the F2 partitions, shown in the low- n region. Note that $P(n)$ is given for integer values of n . Here we have joined the points by a continuous curve to emphasize the beat structure.

It is interesting to note that the beat structure eventually fades out for $n \gtrsim 100,000$ (as

shown in Sec. V), while the oscillations persist even as $n \rightarrow \infty$. Where are these regular oscillations coming from? Consider an integer n that is a sum of squares: $n = m^2 + p^2$. If n itself is a square: $n = q^2$, then the three numbers m, p, q form what is commonly called a Pythagorean triple (PT) of integers (m, p, q) with $m^2 + p^2 = q^2$. Such triples can only occur in square partitions, since Fermat's last theorem [4] asserts that only squares of integers may be written as sums of two (or more) other squares. Since an increasing number of such triples will occur in the F2 partitions with increasing n , it is quite plausible that they reflect themselves in the oscillatory behaviour of the function $P(n)$.

In semiclassical physics [5, 6], oscillatory behavior in the quantum-mechanical density of state of a dynamical system are described by a superposition of the periodic orbits of the corresponding classical system. The quantitative link between the quantum and classical description is called a 'trace formula' [5]. In many examples it has been shown [6] that the gross features of quantum oscillations may be interpreted in terms of the shortest periodic orbits of the system, whose interference often leads to beating patterns. One of the goals of the present paper is to find a semiclassical trace formula for the oscillations in $P(n)$.

As mentioned above, F2 partitions express an integer n as a sum of distinct squares. This is analogous to the distribution of the total energy $E = n = m_1^2 + m_2^2 + \dots$ amongst unrestricted numbers of Fermions in a one-dimensional box whose spectrum is given by the squares of integer quantum numbers m_i (when all scales are set to unity). Thus we can map the F2 partitions onto a dynamical system in which fermions move in a one-dimensional box. This allows us to use the language of dynamical systems, with the notion of 'energy' and its conjugate variable defined in Fourier space, the (time) 'period'. The inverse of the period is then the 'frequency' of the classical 'orbit' in the dynamical system (though all these quantities are dimensionless in the present case). We will demonstrate that the orbits with the frequencies 4 and 5 that occur in the smallest PT (3,4,5) are sufficient to reproduce the beating oscillations in $\delta P(n) = P(n) - P_{as}(n)$ of the F2 partitions for $n \gtrsim 4000$. For smaller n , more orbits – amongst them with frequencies 12 and 13 contained in the PT (5,12,13) – are needed to reproduce $\delta P(n)$, while in the asymptotic domain $n \gtrsim 100,000$, where the beat fades away, the orbits with frequency 4 alone reproduce the correct oscillations.

Our paper is structured as follows. Section II contains our basic definitions and some formal results. Amongst them is an integral representation of $P(n)$ that later serves as a starting point for our semiclassical studies. In Sec. III we focus on the asymptotic smooth

part $P_{as}(n)$. We use the stationary-phase method for not only re-deriving the leading-order asymptotic expression $P_{as}^{(0)}(n)$ given in [1], but also to find saddle-point corrections which lead to a faster convergence of $P_{as}(n)$ to the average of the exact $P(n)$. We show that the limit $P(n)/P_{as}(n) \rightarrow 1$ is practically reached for $n \sim 10,000$.

In Sec. IV we present the Fourier spectrum of $P(n)$. We classify the leading peaks of the F2 spectrum into successive generations with decreasing intensities and observe a dominant presence of pairs of Fourier peaks whose frequencies are related to PTs. This suggests that the main oscillations in $P(n)$ may, indeed, be governed by the smallest PTs.

Finally, in Sec. V, we focus on the oscillating part $\delta P(n)$. Using stationary-phase integration over a few leading saddles in the complex β plane that correspond to the dominating Fourier peaks, we derive a semiclassical trace formula for $\delta P(n)$. The results converge very fast upon including successive generations of orbits. In fact, the exact $\delta P(n)$ is reproduced by the trace formula already for $n \gtrsim 4000$ using only the orbits with the frequencies 4 and 5 appearing in the PT (3,4,5). The rapid oscillations in $\delta P(n)$ have roughly the period of the orbit with the largest amplitude (frequency 4), while the period of the beating amplitude is given by the inverse difference 20 of their frequencies.

In Appendix A we explain details of the saddle-point corrections for the smooth part of the partition density, and in Appendix B we illustrate the stationary-phase integration method in the complex plane as a tool for evaluating asymptotic oscillations for the model case of the Airy function.

II. BASIC DEFINITIONS AND FORMAL RESULTS

A. Unrestricted square partitions

The function $P(n)$ counts the number of ways in which a given integer n can be written as a sum of distinct squares of positive integers m_i :

$$n = \sum_{i=1}^{I_n} m_i^2, \quad m_i \neq m_j \text{ for } i \neq j. \quad (1)$$

Hereby the number I_n of summands is not specified. It may start from $I_n = 1$, in which case m_1 is the largest integer $\leq \sqrt{n}$. The highest I_n is limited by the value of n itself and

may be found from summing the lowest I_n distinct squares, so that

$$\sum_{i=1}^{I_n} i^2 = I_n(I_n + 1)(2I_n + 1)/6 \leq n. \quad (2)$$

This leads for large n to the upper limit

$$I_n \leq (3n)^{1/3} - 1/2 + \mathcal{O}(n^{-1/3}). \quad (3)$$

Each particular sum (1) is called a ‘partition’ of n into squares. The word ‘distinct’ implies that all m_i within each partition must be different. This is analogous to the distribution of single-particle energies among fermions in statistical mechanics at a given total energy. We therefore use the acronym ‘F2’ for these partitions, where ‘F’ stands for fermionic and ‘2’ for squares. The word ‘unrestricted’ specifies the fact that the number I_n in (1) is not fixed. We define $P(0) = 1$ and, trivially, one sees that $P(1) = 1$. The infinite series of numbers given by $P(n)$ for $n = 0, 1, 2, \dots$ is called the series A033461 in the on-line encyclopedia of integer sequences (OEIS) [7]. Its first ten members are 1, 1, 0, 0, 1, 1, 0, 0, 0, 1.

The partition function $Z(\beta)$ for the unrestricted F2 partitions was given in [1] in several forms. We may obtain it as a generating function, which for any given partition $P(n)$ is defined as

$$Z(\beta) = \sum_{n=0}^{\infty} P(n) e^{-n\beta}. \quad (4)$$

For the F2 partitions it becomes (cf. Table 14.1 of [3])

$$Z(\beta) = \prod_{m=1}^{\infty} [1 + e^{-m^2\beta}], \quad (5)$$

which was also used to generate our data base for the $P(n)$ up to $n = 160,000$.

In the following we write the complex variable β as

$$\beta = x + i\tau, \quad (x, \tau \in \mathbb{R}), \quad (6)$$

where x and τ are dimensionless real variables. Note that (5) can be viewed as a fermionic canonical grand partition function with chemical potential $\mu = 0$. Therefore there is no constraint on the average particle number N which may go up to infinity. Its single-particle spectrum is given by integer squares, as for a particle in an infinite square box (with dimensionless energy and spatial units).

The inverse Laplace transform of $Z(\beta)$ yields the partition density $g(E)$:

$$g(E) = \mathcal{L}_E^{-1}[Z(\beta)] = \frac{1}{2\pi i} \int_C Z(\beta) e^{E\beta} d\beta. \quad (7)$$

Here E is a dimensionless real variable. We choose here the symbol E because of its relation to the energy in the context of statistical physics, where $g(E)$ is the level density (or density of states) of a system of independent particles.

The contour C in (7) runs parallel to the imaginary axis τ with a real part $x = \epsilon > 0$, so that we may write

$$g(E) = \frac{1}{2\pi} \int_{-\infty}^{+\infty} Z(\epsilon + i\tau) e^{E(\epsilon + i\tau)} d\tau \quad (\epsilon > 0). \quad (8)$$

The (two-sided) Laplace transform of $g(E)$ gives back the partition function $Z(\beta)$:

$$\mathcal{L}_\beta[g(E)] = \int_{-\infty}^{+\infty} g(E) e^{-E\beta} dE = Z(\beta). \quad (9)$$

Using the form (4), the density of F2 partitions is immediately found to be

$$g(E) = \sum_{n=0}^{\infty} P(n) \delta(E - n), \quad (10)$$

where $\delta(E - n)$ is the Dirac delta function peaked at $E = n$.

In order to recover the $P(n)$ from the partition density (10), we just have to integrate it over a small interval around $E = n$:

$$P(n) = \int_{n-a}^{n+a} g(E) dE, \quad (0 < a < 1). \quad (11)$$

If we choose $a = 1/2$, Eq. (11) corresponds to an averaging of $g(E)$ over a unit interval $\Delta n = 1$ around n . Averaging $g(E)$ over larger intervals ΔE therefore corresponds to averaging the $P(n)$ over some larger interval Δn :

$$\langle g(E) \rangle_{\Delta E} \sim \langle P(n) \rangle_{\Delta n}. \quad (12)$$

This property will be used in Sec. III to evaluate the asymptotic part of $P(n)$.

For our following investigations, we rewrite (5) in the form

$$Z(\beta) = \exp \left\{ \sum_{m=1}^M \ln [1 + e^{-m^2 \beta}] \right\}. \quad (13)$$

In principle M is infinity according to Eq. (5). However, when calculating the partition density $g(E)$ using the Laplace inverse (9) at finite E , we have for the reason given after Eq. (1) the restriction

$$M(E) = [\sqrt{E}], \quad (14)$$

where $[\sqrt{E}]$ denotes the largest integer M contained in \sqrt{E} .

We note that $Z(\beta)$ in (13) has no poles on the right half β plane, including the imaginary axis as long as $M(E)$ is finite. We may therefore shift the contour C onto the imaginary axis (i.e., choose $\epsilon = 0$) and write the inverse Laplace transform (7) as

$$g(E) = \frac{1}{2\pi} \int_{-\infty}^{+\infty} Z(i\tau) e^{iE\tau} d\tau = \frac{1}{2\pi} \int_{-\infty}^{+\infty} \exp \{iE\tau + \ln Z(i\tau)\} d\tau. \quad (15)$$

Since the imaginary part of the integrand above is antisymmetric w.r.t. $\tau = 0$, the result $g(E)$ becomes real, as it must be, and we only need retain the real part of the integral:

$$g(E) = \frac{1}{2\pi} \int_{-\infty}^{+\infty} \mathcal{R}e \exp \{iE\tau + \ln Z(i\tau)\} d\tau. \quad (16)$$

We next define the Fourier transform (FT) of $g(E)$ by

$$\mathcal{F}_\tau[g(E)] = \int_{-\infty}^{+\infty} g(E) e^{-iE\tau} dE = F(\tau). \quad (17)$$

Note that E and τ are a pair of conjugate dimensionless variables. Comparing (9) and (17), we can write $F(\tau)$ as

$$F(\tau) = Z(i\tau), \quad (18)$$

i.e., $F(\tau)$ is given by the values of $Z(\beta)$ along the imaginary axis τ . This is a general property valid for any partition function $Z(\beta)$ which has no poles on or to the right of the imaginary axis. The absolute value of $F(\tau)$, inserting the partition function (13) into (18), becomes

$$|F(\tau)| = \exp \{ \mathcal{R}e \ln Z(i\tau) \}. \quad (19)$$

This Fourier spectrum will be studied numerically in Sec. IV.

B. Integral representation of $P(n)$

We start from the expression (15) for the Laplace inversion of $Z(\beta)$. We now formulate the following **Lemma**: *The Laplace inversion integral (15) limited to the interval*

$\tau \in (-k\pi, +k\pi)$ with $k = 1, 2, \dots$ yields a sum of Bessel functions weighted by $P(n)$ such that its value at $E = n$ is $kP(n)$:

$$g^{(k)}(E) = \frac{1}{2\pi} \int_{-k\pi}^{+k\pi} e^{iE\tau} Z(i\tau) d\tau = k \sum_{n=0}^{\infty} P(n) j_0(k\pi(E - n)). \quad (k = 1, 2, 3, \dots) \quad (20)$$

Proof: For finite k , we use the form (4) of $Z(\beta)$ and the integration yields immediately Eq. (20). Since $j_0(0) = 1$, we get

$$g^{(k)}(E=n) = kP(n), \quad (21)$$

as claimed at the end of the lemma. *q.e.d.*

In the limit $k \rightarrow \infty$, the Bessel functions become delta functions (see, e.g., Schiff [8]):

$$\lim_{k \rightarrow \infty} [kj_0(k\pi(E - n))] = \delta(E - n). \quad (22)$$

Therefore the limit $k \rightarrow \infty$ yields the exact partition density as it should:

$$\lim_{k \rightarrow \infty} g^{(k)}(E) = \sum_{n=0}^{\infty} P(n) \delta(E - n) = g(E). \quad (23)$$

The function $g^{(1)}(E)$ in (20) represents a smooth interpolation curve through the exact values $P(n)$ at $E = n$, which we like to call a ‘Bessel-smoothed’ partition density. It is shown in Figs. 2 and 3.

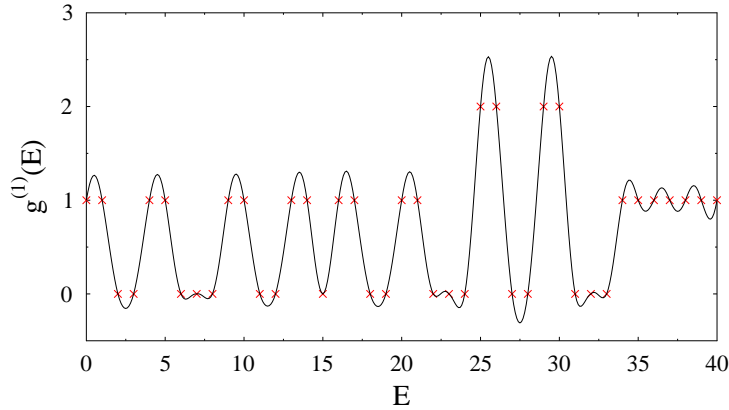


FIG. 2: Bessel-smoothed partition density $g^{(1)}(E)$ (20) (black line) for small energies E . The red crosses at integer values of $E = n$ show the exact values of $P(n)$.

Setting $E = n$ in (20) with $k = 1$, we obtain the following integral representation of $P(n)$:

$$P(n) = \frac{1}{2\pi} \int_{-\pi}^{\pi} \mathcal{R}e e^{in\tau} Z(i\tau) d\tau = \frac{1}{2\pi} \int_{-\pi}^{\pi} \mathcal{R}e \exp \left[in\tau + \sum_{m=1}^{[\sqrt{n}]} \ln \left(1 + e^{-im^2\tau} \right) \right] d\tau. \quad (24)$$

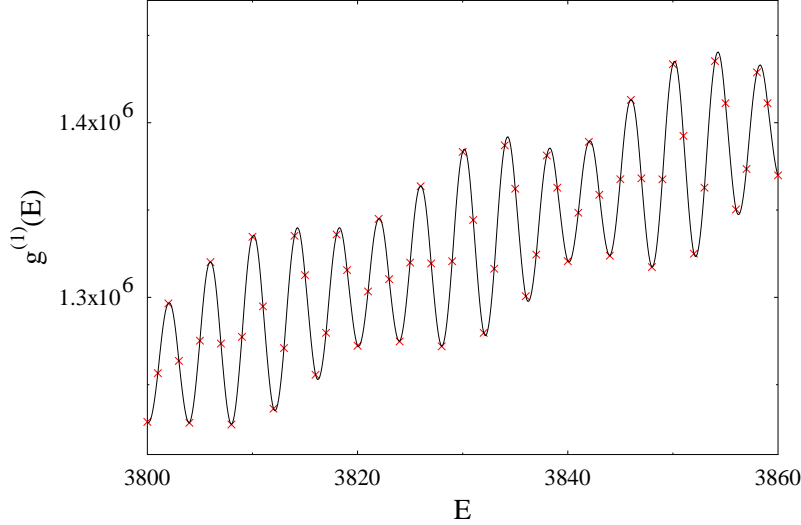


FIG. 3: The same as in Fig. 2 for larger energies E .

This integral formula is one of the central results of our paper. It will be the starting point in Sec. VC for the derivation of a semiclassical trace formula for the oscillations in $P(n)$.

C. A continuous trace formula for $g(E)$

We rewrite the real part of the exponent in (16):

$$g(E) = \frac{1}{2\pi} \int_{-\infty}^{+\infty} \exp[\mathcal{R}e \ln Z(i\tau)] \cos[E\tau + \mathcal{I}m \ln Z(i\tau)] d\tau. \quad (25)$$

Using (19), we obtain the following expression for the partition density:

$$g(E) = \frac{1}{2\pi} \int_{-\infty}^{+\infty} |F(\tau)| \cos[E\tau + \phi(\tau)] d\tau, \quad (26)$$

where the phase function $\phi(\tau)$ is given by

$$\phi(\tau) = \mathcal{I}m \ln Z(i\tau) = \sum_{m=1}^{[\sqrt{E}]} \text{arctg} \left[\frac{-\sin(m^2\tau)}{1 + \cos(m^2\tau)} \right]. \quad (27)$$

In its structure, the expression (26) resembles a semiclassical trace formula (see [6] for more details), with amplitudes given by the Fourier spectrum $|F(\tau)|$, actions by $E\tau$, periods by τ , and phases by $\phi(\tau)$. The difference compared to the standard trace formulae [5, 6] is that here we do not have a discrete sum, but a continuous integral over periodic orbits labeled by the period variable τ . We call Eq. (26) a ‘continuous trace formula’ for the density $g(E)$ of F2 partitions. Note that it is exact, since no approximation has been made

whatsoever in deriving it. It is, in fact, a general result for any level density $g(E)$, provided one knows its Fourier spectrum $|F(\tau)|$ and its Laplace transform on the imaginary axis τ . Unless these ingredients are known analytically, Eq. (26) is of no practical use. The only exact case we found is the example of the one-dimensional harmonic oscillator without zero point energy. It has the single-particle spectrum $E_n = n$ ($n = 0, 1, 2, \dots$) and corresponds to $P(n) = 1$. Its Fourier peaks are at $\tau_k = 2\pi k$ with $\phi(\tau_k) = 0$, so that (26) reproduces the exact trace formula given in [6], eq. (3.40):

$$g_{ho}(E) = 1 + 2 \sum_{k=1}^{\infty} \cos(2\pi k E). \quad (28)$$

Eq. (26) gives us, however, a hint as to how a trace formula with discrete orbits and periods could look like. In Sec. V C we shall use a semiclassical approach for its realization.

III. ASYMPTOTIC EXPANSION OF THE SMOOTH PART OF $g(E)$

In this section we briefly re-derive the leading asymptotic form $P_{as}(n)$ of the square partitions, given already in [1], and then obtain a series of next-to-leading order contributions which yields a faster convergence to the average values of the exact $P(n)$. We closely follow the method used in Refs. [1, 9]. As stated above in (12), averaging over $g(E)$ yields an average of $P(n)$. Therefore the results of the smooth asymptotic part of $g(E)$ can be identified with that of $P(n)$ when E is taken as an integer n .

A. Leading asymptotic form $g_{as}^{(0)}(E)$

We rewrite the inverse Laplace transform in Eq. (7) for the function $g(E)$ in the form

$$g(E) = \mathcal{L}_E^{-1}[Z(\beta)] = \frac{1}{2\pi i} \int_C e^{S(E,\beta)} d\beta, \quad (29)$$

where $S(E, \beta)$ is given by

$$S(E, \beta) = E\beta + \ln Z(\beta). \quad (30)$$

which is often called the ‘entropy’. We now derive the asymptotic smooth part of $g(E)$ by performing the inverse Laplace transform (29) by saddle-point integration. The asymptotic smooth part for large E comes from the neighborhood of a real saddle point in the complex β plane, lying near the imaginary axis. Doing the Laplace integral over such a saddle point by

the method of stationary phase should yield the asymptotic smooth part of $g(E)$. Hereby we can approximate the sum over m in (13) using the Euler-MacLaurin expansion [10], yielding

$$S(E, \beta) \simeq E\beta + \int_0^\infty dq \ln [1 + e^{-q^2\beta}] - \frac{1}{2} \ln(2). \quad (31)$$

Doing the integration [11], we obtain for real $\beta = x$

$$S(E, x) \simeq Ex + \frac{\Gamma(3/2)\eta(3/2)}{\sqrt{x}} - \frac{1}{2} \ln(2), \quad \eta(3/2) = \sum_{l=1}^{\infty} \frac{(-1)^{l-1}}{l^{3/2}}, \quad (32)$$

where $\eta(z)$ is the Dirichlet eta function. To find a real saddle point (SP) x_0 , we have to solve the SP equation

$$S_1(E, x_0) = \left. \frac{\partial S(E, x)}{\partial x} \right|_{x_0} = E - \frac{D}{2x_0^{3/2}} = 0, \quad D = \Gamma(3/2)\eta(3/2) = 0.678093895. \quad (33)$$

Here $S_i(E, x)$ denotes the i -th partial derivative of $S(E, x)$ with respect to x at fixed E . This yields the solution for the SP x_0 at each energy E :

$$x_0(E) = \left[\frac{D}{2E} \right]^{2/3} = \lambda_0 E^{-2/3}, \quad \lambda_0 = (D/2)^{2/3} = 0.486227919. \quad (34)$$

Doing the contour integral over τ parallel to the imaginary axis in the stationary-phase approximation yields

$$g_{as}^{(0)}(E) = \frac{\exp[S(E, x_0)]}{\sqrt{2\pi}|S_2(E, x_0)|} = \sqrt{\frac{\lambda_0}{6\pi}} E^{-5/6} \exp(3\lambda_0 E^{1/3}), \quad (35)$$

so that, using the property (12),

$$P_{as}^{(0)}(n) = \sqrt{\frac{\lambda_0}{6\pi}} n^{-5/6} \exp(3\lambda_0 n^{1/3}). \quad (36)$$

This is the leading-order asymptotic form of $P(n)$ given already in Ref. [1] (where our present λ_0 was called λ_2).

B. Higher-order contributions to $g_{as}^{(0)}(E)$

In Appendix A we derive higher-order saddle-point contributions to the result (35), yielding a better asymptotic form $g_{as}(E)$ up to third order as given in (A24). For the F2 partition counting function, this yields

$$P_{as}(n) = \sqrt{\frac{\lambda_0}{6\pi}} n^{-5/6} e^{3\lambda_0 n^{1/3}} [1 - c_1 n^{-1/3} - c_2 n^{-2/3} - c_3 n^{-1}], \quad (37)$$

with the coefficients c_1 , c_2 , and c_3 given in Eqs. (A25), (A26). In Fig. 4 we show the leading approximation $P_{as}^{(0)}(n)$ (dashed line) and the improved result $P_{as}(n)$ using (37) (solid line). The latter is seen to give an excellent agreement with the average through the exact $P(n)$.

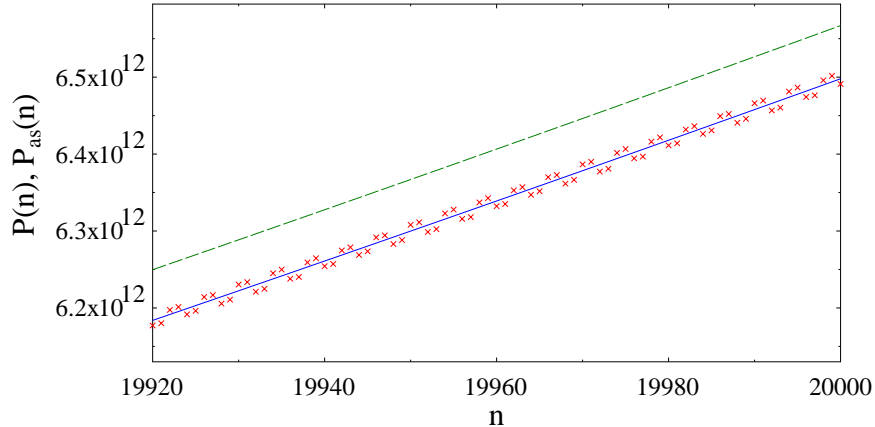


FIG. 4: Exact $P(n)$ by crosses (red), leading-order asymptotic part $P_{as}^{(0)}(n)$ (36) by the dashed (green) line, and corrected asymptotic part $P_{as}(n)$ (37) by the solid (blue) line in the large- n region.

Figure 5 shows that the relative amplitude of the oscillations decreases exponentially with n , as given more quantitatively in Eq. (55) below, and that the ratio $P(n)/P_{as}(n)$ reaches unity at $n \gtrsim 10,000$. The improved asymptotic form (37) thus brings a substantial improvement over the leading-order term $P_{as}^{(0)}(n)$ for which the limit $P(n)/P_{as}(n) \rightarrow 1$ is not reached (see also Ref. [7]).

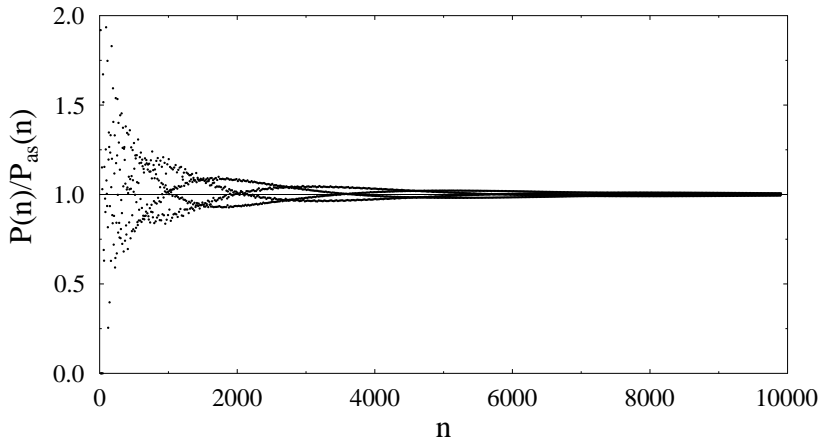


FIG. 5: Ratio $P(n)/P_{as}(n)$ showing that $P_{as}(n)$ in (37) including the SP corrections reaches correctly the average values of $P(n)$ in the large- n limit: $P(n)/P_{as}(n) \rightarrow 1$.

For $n \gtrsim 100,000$ we found that the truncated series with three terms in (37) does not converge fast enough; we will come back to this point at the end of Sec. V C.

IV. FOURIER ANALYSIS OF $g(E)$

In order to understand the oscillating part of $P(n)$ we now investigate the Fourier spectrum Eq. (19) of the F2 partitions. We shall use both forms given in Eqs. (4) and (13) for $Z(\beta)$ and plot the results versus the frequency $f = 2\pi/\tau$.

A. Fourier spectra using Eq. (4)

We first look at the Fourier spectra obtained from (4) with a linear cut-off given by

$$F(f) = \sum_{n=0}^{n_{max}} P(n) e^{-2\pi i n/f} (1 - n/n_{max}). \quad (38)$$

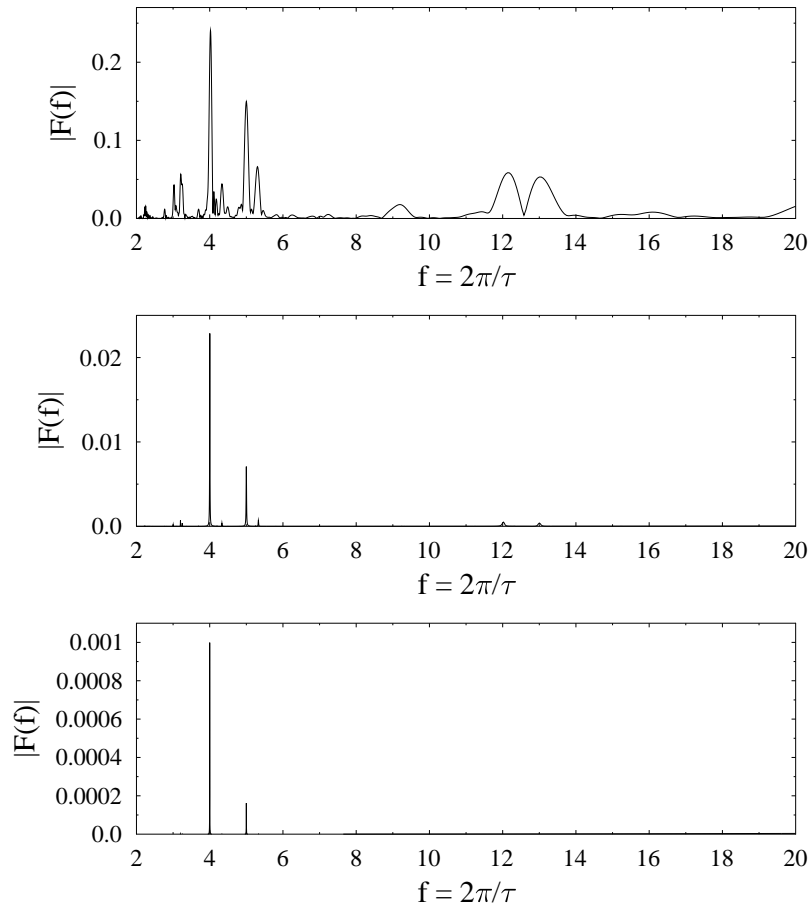


FIG. 6: Fourier spectra $|F(f)|$ using $Z(\beta)$ in (4) versus frequency f . The cut-off of the n sum in (38) is, from top to bottom, $n_{max} = 300, 4000,$ and $20,000$.

Figure 6 shows the results for $|F(f)|$ with, from top to bottom, $n_{max} = 300, 4000,$ and $20,000$ in the region $2 \leq f \leq 20$ (normalized to unit intensity at $f = 1$). The spectra are

clearly cut-off dependent and reveal a varying number of visible frequencies in the different regions of n . For the lowest cut-off, the peaks are becoming more diffuse with increasing f , but we clearly find many more frequencies than for the higher cut-offs. For $n_{max} = 300$ we recognize peaks, with varying intensities, near the frequencies $f = 4, 5, 12,$ and 13 (besides others). Interestingly, these numbers belong to the lowest PTs $(3,4,5)$ and $(5,12,13)$. This gives us a hint that the spectrum of $P(n)$ is dominated by the lowest PTs. For $n_{max} = 4000$, the peaks at $f = 4$ and 5 dominate, while only tiny hints of the other frequencies can be seen. For $n_{max} = 20,000$ no more trace is left of the other frequencies, and the frequency 4 is clearly dominating over $f = 5$.

The tendency that a decreasing number of frequencies is important with increasing n will be confirmed in Sec. V by the semiclassical interpretation of the oscillations in $P(n)$.

B. Fourier spectra using Eq. (13)

Because of the bad resolution of the above spectra for small n , we now investigate the FT spectra that we obtain using Eq. (13) for $Z(\beta)$. Their frequency information is in principle the same, but the peaks turn out to be much cleaner, allowing us to identify their exact frequencies f and to compare their relative intensities.

We first discuss the dependence on the upper limit M of the m summation in (13). We argue that $|F(f)|$ actually is a distribution function with infinite peaks at many integer or rational values of f . It therefore has to be normalized in some suitable way.

1. Normalization of $|F(f)|$

In Fig. 7 we show the intensity of $|F(f)|$ in a close-up near a peak at $f = 5$. Shown are the curves for increasing values of the upper limit M of the m summation, namely for $M = 500, 1000,$ and 5000 (from top to bottom). The horizontal line gives the calculated value 0.7554 of the scaled intensities (see Tab. I below). We see that with increasing M , the curves become narrower, and in the limit $M \rightarrow \infty$, we can take the local spectrum to be a (renormalized) delta function peaked at $f = 5$.

The normalization of the curves in all figures has been chosen in the following way. It is easy to see that for $\tau_k = 2k\pi$ with integer k , the exponential in Eq. (13) becomes unity, so

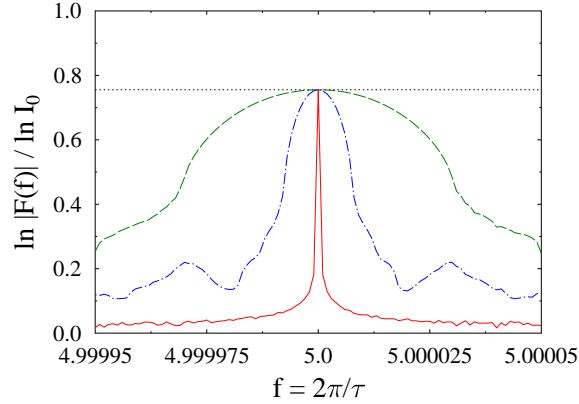


FIG. 7: Close-up of the scaled $\ln |F(f)|$ near the frequency $f = 2\pi/\tau = 5$, shown for $M = 500$ by the dashed (green) line, $M = 1000$ by the dash-dotted (blue) line, and $M = 5000$ by the solid (red) line. The horizontal dotted line gives the theoretical peak height according to Tab. I.

that we obtain $|F(\tau_k)| = \exp(M \ln 2)$. Below we will call the peaks at $\tau_k = 2k\pi$ (i.e. $f_k = 1/k$) the ‘generation 0’ peaks which on a logarithmic scale have the intensity $\ln I_0 = M \ln 2$. In all figures we therefore show the scaled function $\ln |F(f)| / \ln I_0$, so that the generation 0 peaks have the height unity (even if not seen for $f \geq 2$).

2. Numerical Fourier spectra $|F(f)|$

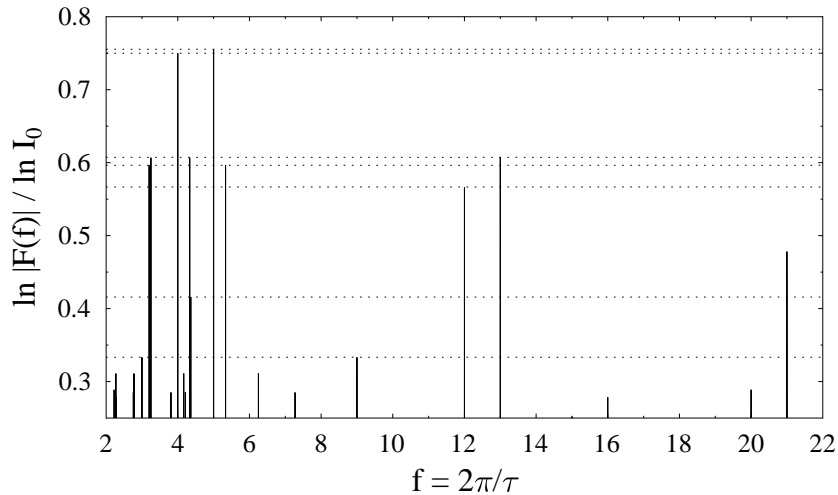


FIG. 8: Scaled Fourier transform $\ln |F(f)|$ of $g(E)$ on a logarithmic vertical scale. The horizontal dashed lines give the calculated relative intensities of the first 10 generations.

Figure 8 shows the Fourier spectrum as a function of the frequency $f = 2\pi/\tau$, plotted for $2 \leq f \leq 22$ with the normalization defined above. The peaks are very sharp. We find peaks

located exactly at $f = 3, 4, 5, 9, 12, 13, 16, 20,$ and 21 ; all other peaks in this interval appear at rational frequencies. We can now classify the peaks into ‘generations’ with decreasing intensities, as listed in Tab. I below. The vertical scale of Fig. 8 was selected such that the peaks of the generations 1 - 10 can be clearly differentiated; their theoretical scaled intensities as given in Tab. I are shown by the horizontal dashed lines.

Figure 9 shows the same for f up to 105. Many more integer-valued frequencies appear. We notice, in particular, the dominating intensities of peak pairs with the frequencies $(4,5)$, $(12,13)$, $(28,29)$, $(36,37)$, $(60,61)$, $(84,85)$, and $(100,101)$. Four of them appear as the largest numbers in PTs, namely in $(3,4,5)$, $(5,12,13)$, $(11,60,61)$ and $(13,84,85)$. The numbers 28, 29 and 101 appear isolated in other PTs.

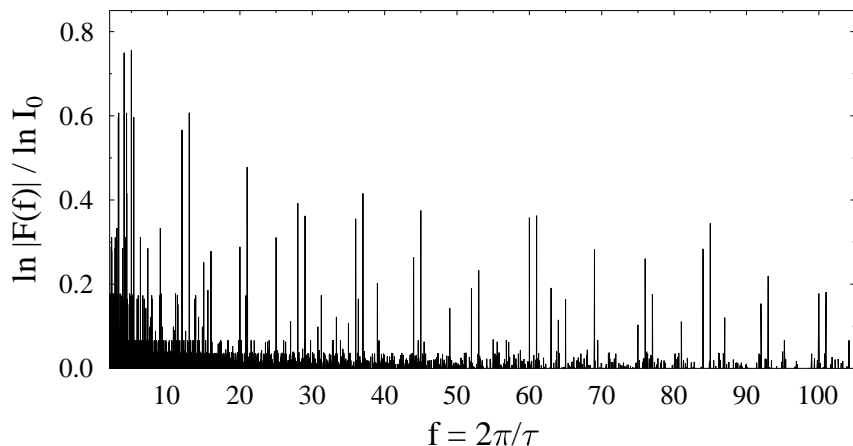


FIG. 9: Same as Fig. 8 over a larger range of the frequency f .

We have thus found a strong evidence that the PTs play a dominant role in the spectrum and hence also the oscillations of $P(n)$. This will, indeed, be confirmed quantitatively by the semiclassical trace formula derived and discussed in Sec. V.

For reasons that become evident in Sec. V, we shall now map the interval $\tau \in (0, 2\pi)$ on the interval $\tau \in (-\pi, +\pi)$. The Fourier spectrum then is symmetric about $\tau = 0$, with the peak pairs of each generation appearing with opposite signs of τ .

Table I presents the first ten generations of Fourier peaks and their properties; for the periods τ_g only the positive values are given. Generation 0 creates the smooth part $P_{as}^{(0)}$, as discussed in Sec. III A. For convenience and brevity, the constants λ_g , μ_g , κ_g , and φ_g are given in the table but will be discussed later in Sec. VB together with the use of the generations 1-10 as ‘orbits’ in a semiclassical trace formula.

g	τ_g	f_g	$\ln I_g/\ln I_0$	λ_g	μ_g	κ_g	φ_g
0	0	1 [†]	1.0	0.48622	0	3.085	0
1	$2\pi/5$	5	0.7554	0.37444	0.0000	4.006	0.0000
2	$2\pi/4$	4	3/4	0.400	0.1999187	3.352	-0.2318
3	$2\pi/13$	13	0.6072	0.30743	0.0000	4.877	0.0000
4	$6\pi/13$	13/3	0.6072	0.30743	0.0000	4.877	0.0000
5	$8\pi/13$	13/4	0.6072	0.30743	0.0000	4.877	0.0000
6	$6\pi/16$	16/3	0.5964	0.3200	-0.154191	4.219	0.2242
7	$10\pi/16$	16/5	0.5964	0.3200	0.154191	4.219	-0.2242
8	$2\pi/12$	12	0.5667	0.3129	0.1606108	4.264	-0.2358
9	$22\pi/48$	48/11	0.4158	0.245	-0.14152	6.502	0.2542
10	$2\pi/3$	3	0.3333	0.2847	0.364242	3.244	-0.4538

TABLE I: Successive generations g of Fourier peaks, their periods τ_g , frequencies f_g and scaled relative intensities I_g . The constants λ_g , μ_g , κ_g , and φ_g are defined and discussed in Sec. V. ([†]The frequency $f_0 = 1$ corresponds to $\tau = 2\pi$ which also belongs to generation 0.)

We should note that there exist further generations (with frequencies 9, 9/2, and 9/4) that have the same intensities as generation 10. Their contributions to the trace formula (53) are, however, negligible. We have listed the generation 10 here mainly because its frequency 3 belongs to the PT (3,4,5).

We also point out that the ordering of the generations is done here according to the decreasing intensities $\ln I_g/\ln I_0$. In Sec. VC we shall see that the semiclassical amplitudes $A_g(n)$ of the ‘orbits’ appearing in the trace formula (53) follow a somewhat different ordering, in agreement with the results in Fig. 6 where the peaks with $f = 4$ (generation 2) have a higher intensity than those with $f = 5$ (generation 1).

V. DERIVATION OF A TRACE FORMULA FOR $\delta P(n)$

In this section we derive a semiclassical trace formula for the oscillating part of $P(n)$. The main idea of our approach is that asymptotic expressions of oscillating functions can be found from stationary-phase integration over complex saddles in the β plane. As shown in Sec. III A, the asymptotic smooth part $P_{as}(n)$ is obtained from the real saddle point x_0 given in (34). This technique has been used, e.g., by Balazs *et al.* [13] to find both smooth and oscillating asymptotic expressions for integrals of the Airy function. We shall illustrate this method in Appendix B for the Airy function itself.

We start from the integral representation (24) of $P(n)$ for which the integration along the τ axis from $-\pi$ to $+\pi$ (contour C) yields the exact $P(n)$ for all n . Since the integrand has no singularities for $x > 0$, we may deform the contour arbitrarily, keeping its end points fixed. We choose it to pass over the most important saddles in the complex β plane corresponding to the leading Fourier peaks, and then use stationary-phase integration locally at each saddle.

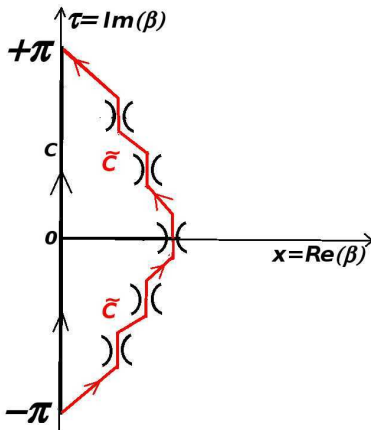


FIG. 10: Schematic plot of the contour for the integral (24). The exact contour C (going from $-\pi$ to $+\pi$ along the τ axis) is deformed into a new contour (red) \tilde{C} which goes over some selected saddles in the complex β plane.

Figure 10 shows a sketch of the situation in the complex β plane, with the deformed contour \tilde{C} chosen to pass over 5 representative saddles. The exact path between the saddles does not matter, since we will only collect the local contributions near each saddle in the stationary-phase approximation. While the real saddle yields the smooth $P_{as}(n)$ as shown in Sec. III A, the complex saddles will yield an approximation for the oscillating part $\delta P(n)$.

A. Saddle points in the complex β plane

Scanning the complex β plane for the function $\mathcal{R}e S(E, \beta)$ in (30) using Eq. (13), we observe that for each of the dominant Fourier peaks listed in Tab. I, there exists a saddle at a stationary point with τ close to the value τ_g listed there. We illustrate this in the following three figures for the generations 0, 1, and 2, with contour plots of the function $\mathcal{R}e S(E, \beta)$ (evaluated here at $E = 40$) in the complex β plane.

Figure 11 shows the real saddle at $\tau_0 = 0$ which was used in Sec. III A to derive the asymptotic function $P_{as}(n)$; the position of the saddle point x_0 axis is given in (34).

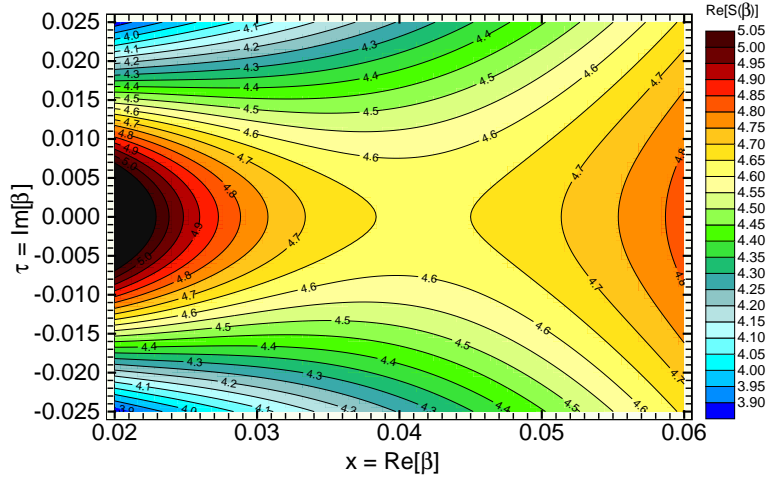


FIG. 11: Contour plot of the function $\mathcal{R}e S(E, \beta)$ in (30), evaluated at $E = 40$, in the saddle-point region of generation 0 at $\tau = 0$.

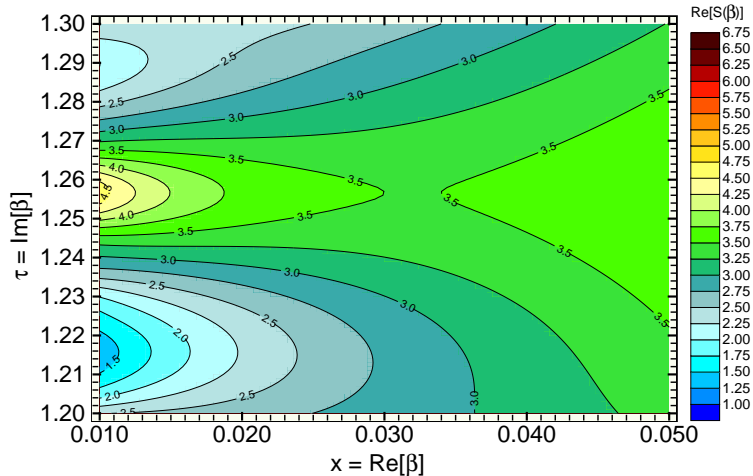


FIG. 12: Same as Fig. 11 for generation 1 at $\tau_1 = 2\pi/5$.

Figure 12 shows one of the saddles of generation 1, lying approximately at $\tau_1 = 2\pi/5$. Note that for generations 0 and 1, the path of steepest descent appears to be parallel to the imaginary axis. This is, however, analytically true only for the real saddle, as will be discussed in the following subsection.

Figure 13 shows one of the saddles of generation 2, lying somewhat below $\tau_2 = 2\pi/4$. The precise value of τ_2 at the saddle is energy dependent and given in Eq. (44) below. The path of steepest descent here is tilted with respect to the τ axis by an angle α_2 which leads to the Maslov index φ_2 defined in Eq. (52) below.

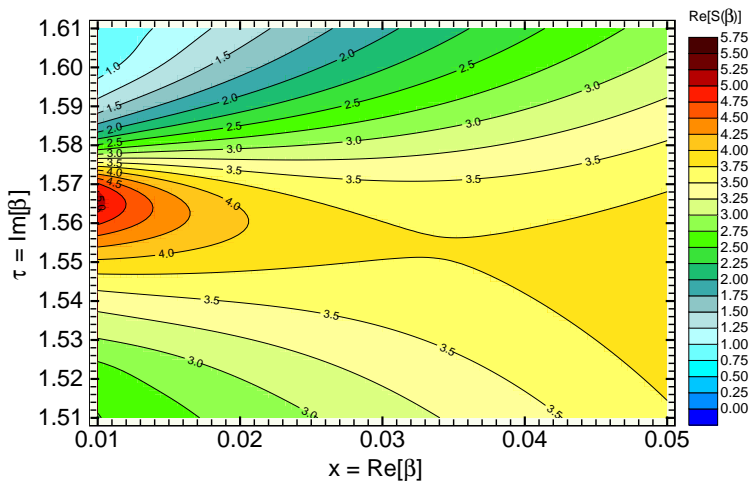


FIG. 13: Same as Fig. 11 for generation 2 at $\tau_2 \sim 2\pi/4$. Note that, different from the two previous cases, the saddle here is tilted with respect to the x and τ axes.

What we see in these three examples can be summarized as follows. From each of the dominant Fourier peaks listed in Tab. I (and for many more), a ridge with a conditional maximum of $S(E, \beta)$ in the τ direction descends from its position on the τ axis (where it corresponds to a peak that diverges for $M \rightarrow \infty$ as discussed in Sec. IV B 1) towards the right, i.e., in the x direction. Eventually it will deviate from the x direction (except for the generations 0, 1, and 3-5) and form a saddle at some value $x_g(E)$. The exact position $\beta_g(E) = x_g(E) + i\tau_g(E)$ of the saddle point (SP) of each generation (as a function of energy E) has to be found by solving the SP equations discussed next.

B. Solutions of the complex saddle-point equations

When integrating over a saddle by the method of steepest descent, one chooses the direction in which the real part of the entropy function $S(E, \beta)$ in (29) has its steepest maximum. This yields a rapidly oscillating phase which tends to cancel all contributions except close to the SP where the phase becomes stationary (hence the alternative name ‘stationary-phase approximation’). Near the SP β_0 , the integrand may be approximated by a Gaussian integral that can be evaluated exactly if the curvature of $\mathcal{R}e S(E, \beta)$ at β_0 is known. While this integral yields a smooth semiclassical amplitude as a function of E (as in Sec. III A), the imaginary part $\mathcal{I}m S(E, \beta)$ at β_0 yields an oscillatory function of E if τ_0 is not zero.

The saddles are thus determined by the stationary condition $\partial S(E, \beta)/\partial\beta|_{\beta_0} = 0$ in the complex β plane, which yields two equations. Using (30) and (13) we find from the real part

$$E - \frac{1}{2} \sum_m m^2 \frac{[\exp(-m^2 x_0) + \cos(m^2 \tau_0)]}{[\text{Cosh}(m^2 x_0) + \cos(m^2 \tau_0)]} = \left. \frac{\partial}{\partial x} \mathcal{R}e S(E, \beta) \right|_{\beta_0} = 0, \quad (39)$$

and from the imaginary part

$$-\frac{1}{2} \sum_m m^2 \frac{\sin(m^2 \tau_0)}{[\text{Cosh}(m^2 x_0) + \cos(m^2 \tau_0)]} = \left. \frac{\partial}{\partial \tau} \mathcal{R}e S(E, \beta) \right|_{\beta_0} = 0. \quad (40)$$

These equations may be transformed into a more symmetrical form, involving double sums

$$E = \sum_m m^2 \sum_{k=1}^{\infty} (-1)^{k+1} e^{-km^2 x_0} \cos(km^2 \tau_0), \quad (41)$$

$$0 = \sum_m m^2 \sum_{k=0}^{\infty} (-1)^k e^{-km^2 x_0} \sin(km^2 \tau_0). \quad (42)$$

We were not able to solve these SP equations analytically, except for the case of the real saddle at $\tau_0 = 0$ for generation 0. In this case, (40) and (42) are trivially fulfilled for all x_0 since $\sin(m^2 \tau_0) = 0$ for all m (and k). For (39) we could then use the Euler-MacLaurin approximation (replacing the m sum by an integral, see Sec. III A) with the result given in (34). In the same spirit, we found that our numerical solutions of the SP equations for all generations g could be very accurately fitted by the equations

$$x_0^{(g)}(E) = \lambda_g E^{-2/3}, \quad (43)$$

$$\tau_0^{(g)}(E) = \pm \tau_g \mp \mu_g E^{-2/3}, \quad (44)$$

with the values of λ_g and μ_g given in Tab. I. For the generation 0, μ_0 is exactly zero. For generations 1 and 3-5, μ_g is zero within the numerical accuracy of the constants given in the table. The entropies S at the saddle points could be fitted by

$$\mathcal{R}e S(E, \beta_0) = 3\lambda_g E^{1/3} - \ln(2)/2. \quad (45)$$

$$\mathcal{I}m S(E, \beta_0) = \pm E\tau_g \mp 3\mu_g E^{1/3}. \quad (46)$$

Note that the last term in (46) contains a contribution $\phi_g(E)$ defined by

$$\phi_g(E) = \mathcal{I}m \ln Z(\beta_g) = \sum_m \text{arctg} \left\{ \frac{-\exp[-m^2 x_0^{(g)}(E)] \sin[m^2 \tau_0^{(g)}(E)]}{1 + \exp[-m^2 x_0^{(g)}(E)] \cos[m^2 \tau_0^{(g)}(E)]} \right\}, \quad (47)$$

which is the analogue of the phase $\phi(\tau)$ in (27) but evaluated here at the complex saddles $\beta_g(E)$. It was numerically found to be well approximated by

$$\phi_g(E) = \mp 2\mu_g E^{1/3}. \quad (48)$$

For the determination of the direction of steepest descent, we proceed as follows. From a given SP (x_o, τ_0) , we define a straight line in the direction α by

$$\beta(r, \alpha) = (x_o + i\tau_0) + r e^{i\alpha}. \quad (49)$$

We then calculate for each α the curvature along r by

$$K_r(E, \alpha) = \mathcal{R}e \left. \frac{\partial^2 S(E, \beta(r, \alpha))}{(\partial r)^2} \right|_{E, \alpha}. \quad (50)$$

This becomes a periodic function whose minimum $\alpha_g \in (0, 2\pi)$ for each generation yields the direction of steepest descent with a maximum absolute value of the (negative) curvature. The resulting K_r could then be numerically fitted by the equation

$$K_r(E, \alpha_g) = -\kappa_g E^{5/3}, \quad (51)$$

with the values κ_g given in Tab. I. For a SP at τ_g with phase α_g , the symmetry partner at $-\tau_g$ has the phase $\pi - \alpha_g$ due to the antisymmetry of $S(E, \beta)$ with respect to the real axis.

All the above functions with the constants in Tab. I, representing the solutions of the SP equations (39) and (40), will henceforth only be used for integer values of the energy variable $E = n$. It remains a challenge for future research to find analytical expressions for these constants.

C. semiclassical trace formula for $\delta P(n)$

We are now equipped for doing the approximate Gaussian integrals over the complex saddles which go exactly like it is explained in Appendix B. Hereby for the symmetry partners of each generation the phases $\exp[i\tau_0^{(g)}(E = n)]$ in (44) and $\phi_g(E = n)$ in (48), together with the phases $\pm \exp(\pm i\alpha_g)$ coming from the Gaussian integrals along r using (49), combine to $2 \cos[n\tau_g - 3\mu_g n^{1/3} + \varphi_g]$, with the constant Maslov index φ_g given by

$$\varphi_g = \alpha_g - \pi/2, \quad (52)$$

which is also listed in Tab. I. We thus arrive at the semiclassical trace formula for $\delta P(n)$

$$\delta P(n) = \sum_{\tau_g > 0} A_g(n) \cos [n\tau_g - 3\mu_g n^{1/3} + \varphi_g], \quad (\tau_g \neq 2\pi k, \quad k = 1, 2, 3, \dots) \quad (53)$$

which is the central result of our paper. Hereby the amplitudes $A_g(n)$ are given by

$$A_g(n) = \frac{2}{(4\pi\kappa_g)^{1/2}} n^{-5/6} e^{3\lambda_g n^{1/3}}. \quad (54)$$

Note that $A_0(n)$ is identical with $P_{as}^{(0)}(n)$ given in (36).

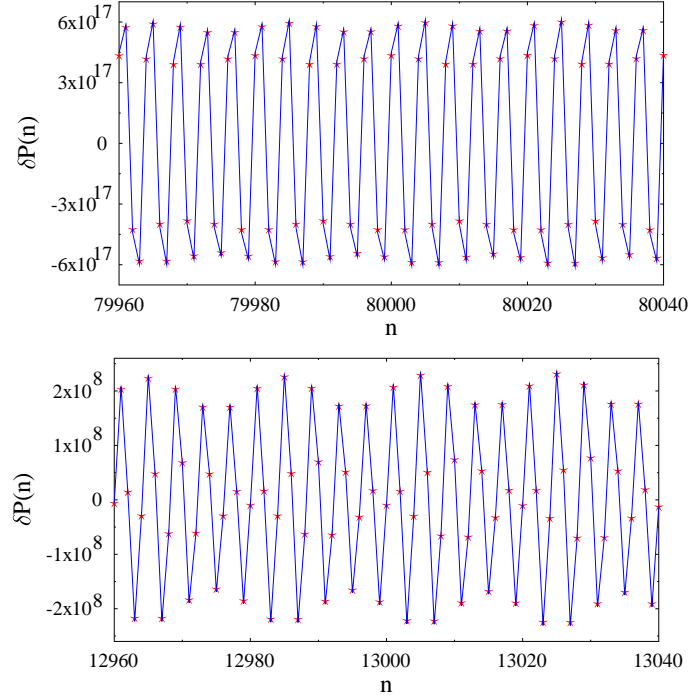


FIG. 14: Result of the trace formula (53), shown by blue lines, versus the exact $\delta P(n) = P(n) - P_{as}(n)$, shown by red stars, in two regions of large n .

Figs. 14 and 15 show the results of the trace formula (53) by blue lines, compared to the exact $\delta P(n) = P(n) - P_{as}(n)$ (red stars) in four ranges of n . The agreement between the two curves is excellent in all regions of n , the semiclassical results reproducing perfectly both the rapid oscillations of the exact $\delta P(n)$ and their beating amplitude.

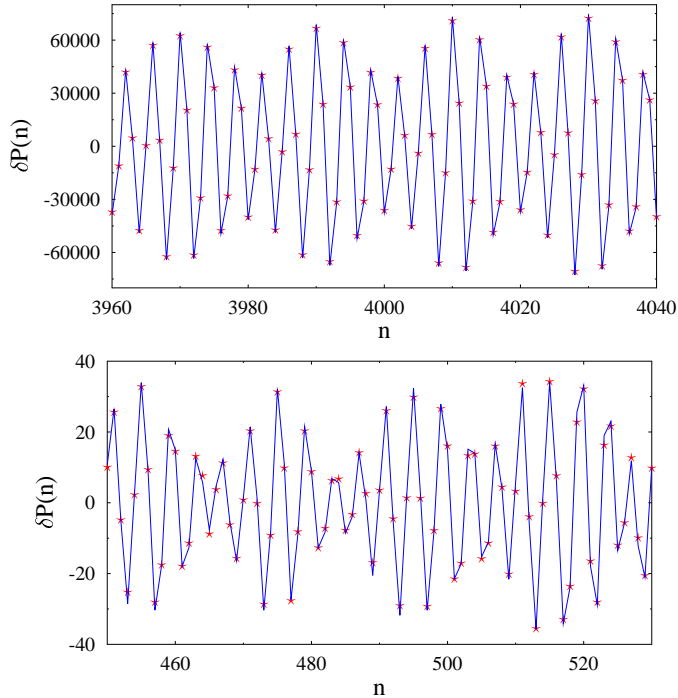


FIG. 15: Result of the trace formula (53), shown by blue lines, versus the exact $\delta P(n) = P(n) - P_{as}(n)$, shown by red stars, in two regions of small n .

In the calculations for these results, the generations 1-10 have been included. However, nothing changes visibly in the results for $n \gtrsim 4000$ if we only include the two leading generations 1 and 2. While this might be a surprise at first sight, it can be explained by the values of the constant λ_g which regulate the exponential growth of the amplitudes $A_g(n)$. These are clearly higher for generations 1 and 2 than for the others.

The relative weights of the generations can be understood from Fig. 16, where we plot the amplitudes $A_g(n)$ on a logarithmic scale. The long-dashed top line gives the amplitude of generation zero, which is identical with $P_{as}^{(0)}(n)$. The solid (s) and short-dashed (s-d) lines give, from top to bottom, the amplitudes of the generations 2 (s), 1 (s), 6+7 (s-d), 3+4+5 (s), 8 (s-d), 10 (s), and 9 (s-d). Note that these amplitudes follow a slightly different ordering than that of the generations listed in Tab. I. The amplitudes of the generations 3 and higher are seen to be smaller than those of generations 1 and 2 by 2-3 orders of magnitudes for

$n \gtrsim 5000$. These in turn are smaller than $P_{as}(n)$ by 2-3 orders of magnitude, demonstrating the relative smallness of the oscillating part.

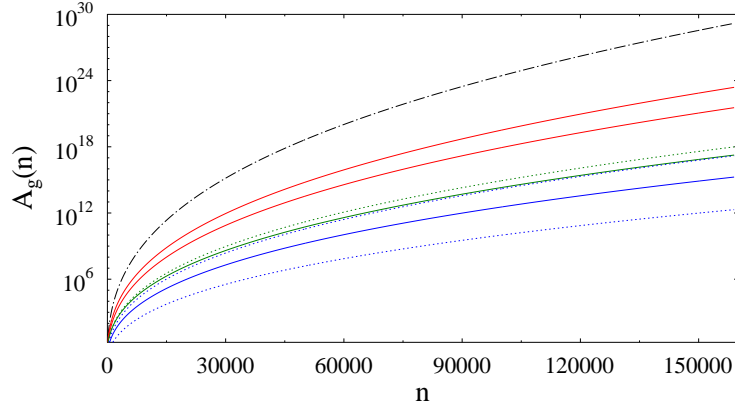


FIG. 16: semiclassical amplitudes $A_g(n)$ for the generations (from top to bottom) 0, 2, 1, 6+7, 3+4+5, 8, 10, 9 (see text for details).

The relative importance of the higher generations around $n \sim 80$ can be studied in Fig. 17. Even here, the generations 1 and 2 produce the essential beating part of $\delta P(n)$. The inclusion of higher generations successively improves the semiclassical values of $\delta P(n)$, although their contributions are rather small and the convergence to the exact values is not as good as for $n \gtrsim 500$. Together, these two figures demonstrate the overall rapid convergence of the trace formula upon summing over the generations g .

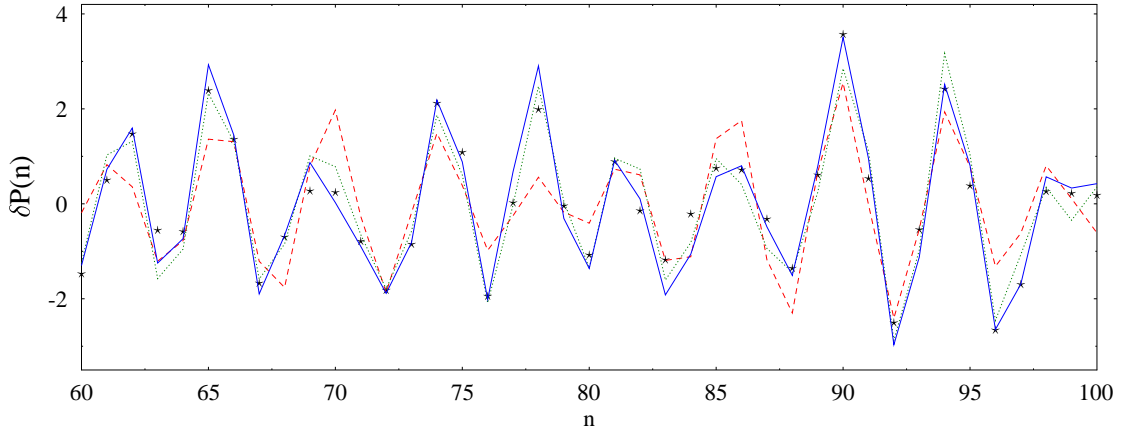


FIG. 17: Result of trace formula (53) around $n = 80$ for increasing numbers of generations included. Dashed line (red): generations 1 and 2; dotted line (green): generations 1-7; solid line (blue): generations 1-10. The stars (black) show the exact $\delta P(n)$.

We conclude that the oscillations in $\delta P(n)$ are dominated everywhere by the orbits of generations 1 and 2 with frequencies 4 and 5, which are members of the PT (3,4,5). The

contributions from all higher generations are practically negligible for $n \gtrsim 4000$ and still very small around $n \sim 500$.

In order to understand the beat structure, one must realize that when changing the variable E to n and studying $\delta P(n)$ as a function of n , the roles of the periods τ_g and frequencies $(2\pi/\tau_g)$ interchange their roles. The terms $\cos(n\tau_g + \dots)$ in (53) have, as functions of n , the (approximate) periods $2\pi/\tau_g$ and hence frequencies τ_g . In the region where the beat structure is dominant, the period of the rapid oscillations is roughly that of the orbit with the largest amplitude[†] (i.e., τ_2 with frequency 4), while the beat comes from the difference in their frequencies: the period $\Delta n = 20$ of the beat is nothing but one over the inverse frequency difference $1/f_2 - 1/f_1 = 1/4 - 1/5 = 1/20$.

For $n \gtrsim 100,000$, the beat structure fades away and the oscillations are practically given by the orbits of frequency 4 alone, as shown in Fig. 18 for n near 160,000. The exact values $\delta P(n)$, shown by the stars, exhibit practically no more beating amplitude. This is due to the fact that the amplitude of generation 2 here is nearly 2 orders of magnitude larger than that of generation 1.

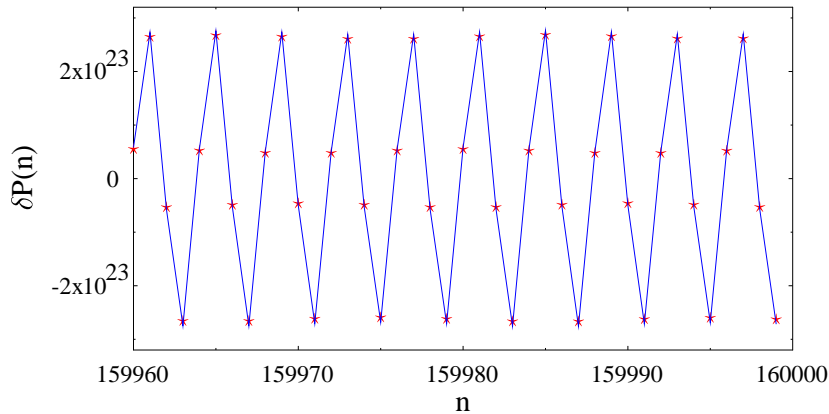


FIG. 18: Result of (53), shown by the blue line, using only the pair of orbits of generation 2 (with $f_2 = 4$), in the region near $n = 160,000$. The exact $\delta P(n) = P(n) - P_{as}(n)$ are shown by the red stars. Note that the beat structure in the exact $\delta P(n)$ has practically disappeared.

[†]The superposition of two cos functions: $a_1 \cos(x_1) + a_2 \cos(x_2)$ with different periods and similar but not equal amplitudes $a_1 > a_2$ yields a beat structure, where the rapid oscillation is governed by the period of the component with the larger amplitude (i.e. a_1). (Only for $a_1 = a_2$ the rapid oscillation has the average period of the two components.)

From this result we can give the rate of disappearance of the relative oscillations as

$$\left| \frac{\delta P(n)}{P_{as}(n)} \right| \sim A_4/A_0 \sim 2\sqrt{\kappa_0/\kappa_2} e^{-3(\lambda_0-\lambda_2) n^{1/3}} \sim 1.9187 e^{-0.25866 n^{1/3}} \quad \text{for } n \rightarrow \infty. \quad (55)$$

In the region $n \gtrsim 100,000$, the truncated series of three SP corrections in (37) does not converge fast enough; this shows up in the numerical results by a slight asymmetry of the numerical $\delta P(n)$ with respect to its average which ought to be zero. We found that a renormalized value $\tilde{c}_3 = 0.025$ of the coefficient c_3 given in (A26) makes up for this asymmetry, yielding with (37) a correct average value $P_{as}(n)$ for all n up to the limit $n = 160,000$ of our data base.

The above results, demonstrating the absolute dominance of the $f = 4$ orbit for $n \rightarrow \infty$, the leading role of the orbits with $f = 4$ and $f = 5$, creating the beating pattern, in the range $4,000 \lesssim n \lesssim 100,000$, and the role of other orbits with higher frequencies in the range $100 \lesssim n \lesssim 4,000$, are in perfect agreement with the Fourier transforms shown in Fig. 6, which were obtained using Eq. (38) with the corresponding cut-offs in the n summation.

VI. SUMMARY

We have investigated the number $P(n)$ of partitions of an integer n into sums of distinct squares (here called F2 partitions) using semiclassical and quantum statistical methods. After some formal definitions in Sec. II leading to the integral representation (24) of $P(n)$, we have in Sec. III derived the asymptotic smooth function $P_{as}(n)$ using the stationary-phase method like in Refs. [1, 9], obtaining not only its leading part but also higher-order contributions from the so-called saddle-point corrections which lead to the correct limit $P(n)/P_{as}(n) \rightarrow 1$ for $n \gtrsim 10,000$. A general method for obtaining the latter for arbitrary systems is given in App. A. The smooth part $P_{as}(n)$ is then used to define the oscillating part as $\delta P(n) = P(n) - P_{as}(n)$.

The oscillations in $\delta P(n)$, with a prominent beat structure for $n \leq 100,000$, have been analyzed in Sec. IV through the Fourier spectrum of the F2 partition density. The most prominent frequencies were found to be integer valued and belong to the lowest Pythagorean triples (PTs) of integers (m, p, q) with $m^2 + p^2 = q^2$, namely (3,4,5) and (5,12,13). Several pairs (p, q) of higher PTs (m, p, q) can also clearly be seen in the Fourier spectrum. We recall that such triples can only occur in square partitions, since Fermat's last theorem [4] asserts

that only squares of integers may be written as sums of two (or more) other squares. It is therefore a particularity of the F2 partitions that the presence of PTs causes the beating oscillations; our Fourier spectra give a clear evidence of this PT dominance.

In the semiclassical theory of quantum densities of states, oscillations are related to sums over periodic functions whose arguments involve the actions of classical periodic orbits [5, 6]. This has been born out quantitatively for the ‘dynamical system’ of F2 partitions in Sec. V, in which we have derived a semiclassical trace formula for $\delta P(n)$ by exploiting the analytical structure of the partition function $Z(\beta)$ (13) in the complex plane. We have evaluated the exact integral (24) for $P(n)$ approximately by deforming the integration contour so as to pass over some selected saddles in the complex β plane, corresponding to the most prominent Fourier peaks, and by locally using stationary-phase integration over these saddles. This leads to the trace formula (53) as the central result of our paper.

The numerical results of (53) reproduce the exact $\delta P(n)$ very accurately all the way from $n \sim 500$ to the upper limit $n = 160,000$ of our data base. For the smallest n , up to 10 generations of orbits – some of them with frequencies belonging to the PT (5,12,13) – have been included to reach good agreement. For $n \gtrsim 4000$, $\delta P(n)$ is completely determined by the orbits with the frequencies 4 and 5 belonging to the smallest PT (3,4,5). The period of the rapid oscillations is hereby governed by the orbits with the larger amplitude (generation 2, frequency $f_2 = 4$), while the beat period $\Delta n = 20$ is one over their inverse frequency difference: $1/f_2 - 1/f_1 = 1/4 - 1/5 = 1/20$. The contributions from all higher generations are negligible for $n \gtrsim 4000$, and still very small around $n \sim 1000$. For $n \gtrsim 100,000$, the beat structure fades away and the oscillations are given by the orbits of frequency 4 alone.

In combination with the Fourier spectra, these results demonstrate an important role of PTs in establishing the beating oscillations in the F2 partitions $P(n)$. In some preliminary statistical studies, we have counted the number $I_N(n)$ of pairs of integers belonging to PTs present in distinct square partitions $P_N(n)$ restricted to N summands. We found that for $N \gtrsim 20$, the functions $I_N(n)$ exhibit the same oscillations as those in the unrestricted F2 partitions $P(n)$ and the Fourier spectra of the $P_N(n)$ are practically identical with those shown in this paper. Further research along these lines is planned.

R.K.B. and M.B. are grateful to the IMSc, Chennai, for its hospitality and excellent working conditions during the initial stages of this work. R.K.B., J.B., and M.V.N. sincerely thank Lis Brack-Bernsen for excellent hospitality in Matting where an important part of this

work was done. Finally M.V.N. acknowledges the peaceful atmosphere in Apollo Hospitals (OMR), Chennai, where parts of the manuscript were completed.

-
- [1] Muoi N. Tran *et al.*, Ann. Phys. (N.Y.) **311**, 204 (2004).
 - [2] G. H. Hardy and S. Ramanujan, Proc. London Math. Soc. 2, XVII:75 (1918).
 - [3] T. M. Apostol: *Introduction to Analytic Number Theory* (Berlin, Springer International Edition, 1989), p. 304.
 - [4] D. Castelvecchi: *Fermat's Last Theorem earns Andrew Wiles the Abel Prize*, Nature **531**, 287 (17 March 2016).
 - [5] M. C. Gutzwiller, J. Math. Phys. **12**, 343 (1971);
R. Balian and C. Bloch, Ann. Phys. (N.Y.) **69**, 76 (1972);
M. V. Berry and M. Tabor, Proc. R. Soc. Lond. A **349**, 101 (1976).
 - [6] M. Brack and R. K. Bhaduri: *semiclassical Physics* (Bolder, Westview Press, 2003).
 - [7] *The On-Line Encyclopedia of Integer Sequences (OEIS)*: <<http://oeis.org/>>.
 - [8] L. L. Schiff: *Quantum Mechanics*, 3rd edition (McGraw-Hill 1968).
 - [9] J. Bartel, R. K. Bhaduri, M. Brack, and M. V. N. Murthy, Phys. Rev. E **95**, 052108 (2017).
 - [10] M. Abramowitz and I. A. Stegun: *Handbook of Mathematical Functions*, 9th printing (New York, Dover, 1972).
 - [11] I. S. Gradshteyn and I. M. Ryzhik: *Table of Integrals, Series, and Products* (New York, Academic Press, 5th edition, 1994).
 - [12] M. R. Hoare, J. Chem. Phys. **52**, 5695 (1970);
A. Jelovic, Phys. Rev. C **76**, 017301 (2007).
 - [13] N. L. Balazs, H. C. Pauli and O. B. Dabbousi, Math. of Comp., Vol. **33** No. 145 (1979) pp. 353-358.

Appendix A: Stationary-phase integration: Higher-order contributions

In this appendix we briefly resume the method of stationary-phase integration including saddle-point corrections at higher order for a real saddle, closely following Ref. [12].

Consider an integral of the form

$$g(E) = \frac{1}{2\pi i} \int_{\epsilon-i\infty}^{\epsilon+i\infty} d\beta e^{S(E,\beta)}, \quad (\text{A1})$$

where $S(E, \beta)$ is the entropy function defined in (30). In order to derive an asymptotic form $g_{as}(E)$ valid for large E , we use the method of stationary phase by expanding the exponent $S(E, \beta)$ around a saddle point (SP). For convenience we denote the derivatives of S here by

$$S_n(\beta) = \frac{\partial^n S(E, \beta)}{\partial \beta^n}, \quad (\text{A2})$$

omitting the argument E which for the present development is just a parameter. We assume that there exists a real SP β_0 so that

$$S_1(\beta_0) = 0, \quad \beta_0 > 0. \quad (\text{A3})$$

Taylor expanding the entropy $S(E, \beta)$ about β_0 we have

$$S(E, \beta) = S(E, \beta_0) + S_2(\beta_0) \frac{(\beta - \beta_0)^2}{2} + R(\beta), \quad (\text{A4})$$

where

$$R(\beta) = \sum_{m=3}^{\infty} S_m(\beta_0) \frac{(\beta - \beta_0)^m}{m!}. \quad (\text{A5})$$

Hence we obtain an asymptotic form

$$g_{as}(E) = \frac{e^{S(E,\beta_0)}}{2\pi i} \int_{\epsilon-i\infty}^{\epsilon+i\infty} d\beta e^{S_2(\beta_0) \frac{(\beta-\beta_0)^2}{2}} e^{R(\beta)}. \quad (\text{A6})$$

Without loss of generality we can choose $\epsilon = \beta_0$ and define the variable

$$u = (\beta - \beta_0)/i. \quad (\text{A7})$$

Expanding the exponential of R under the integral we find

$$g_{as}(E) = \frac{e^{S(\beta_0)}}{2\pi} \int_{-\infty}^{\infty} du e^{-\frac{1}{2} S_2(\beta_0) u^2} \left[1 + R(u) + \frac{R^2(u)}{2!} + \frac{R^3(u)}{3!} + \dots \right]. \quad (\text{A8})$$

This leads to Gaussian integrals over u such that only even powers of u contribute, leaving $g(E)$ real as it should be. Collecting the even powers of u , we get

$$g_{as}(E) = \frac{e^{S(\beta_0)}}{2\pi} \int_{-\infty}^{\infty} du e^{-\frac{1}{2}S_2(\beta_0)u^2} \left[1 + \sum_{m=2}^{\infty} (-1)^m u^{2m} \sum_{\{k\}} \prod_{i=1}^k \left(\frac{S_{n_i}}{n_i!} \right)^{m_i} \left(\frac{1}{m_i!} \right) \right], \quad (\text{A9})$$

where the sum over $\{k\}$ implies the following constraints:

$$2m = m_1 n_1 + m_2 n_2 + \cdots + m_k n_k, \quad n_i \geq 3, \quad k \geq 1, \quad (\text{A10})$$

which is the allowed number of partitions of $2m$ into k parts with repetitions allowed through the power m_i . All such partitions contribute at order $2m$ in u . The integration is now straightforward, since the basic integrals needed are simply

$$\int_{-\infty}^{\infty} du e^{-au^2} u^{2m} = \frac{(2m-1)!!}{2^m a^m} \sqrt{\pi/a}. \quad (\text{A11})$$

With this we obtain a result that formally contains SP corrections to all orders:

$$g_{as}(E) = \frac{e^{S(\beta_0)}}{\sqrt{2\pi S_2(\beta_0)}} \left[1 + \sum_{m=2}^{\infty} (-1)^m \frac{(2m-1)!!}{S_2^m} \sum_{\{k\}} \prod_{i=1}^k \left(\frac{S_{n_i}}{n_i!} \right)^{m_i} \left(\frac{1}{m_i!} \right) \right]. \quad (\text{A12})$$

This is a series with $1/S_2^2$ as the expansion parameter. Even though this result is written to all orders, we note that it is an asymptotic series obtained by Taylor expansion of the entropy around a point $\beta = \beta_0$. Hence, depending on the system under consideration, truncation of the series must be handled with care.

We now use Eq. (A12) to obtain the SP corrections to the asymptotic F2 partition density given in (35). To leading order we have

$$S(E, \beta) = \beta E + \frac{D}{\sqrt{\beta}} - \frac{1}{2} \ln(2), \quad (\text{A13})$$

and at the real SP β_0 we have

$$E = \frac{D}{2\beta_0^{3/2}}, \quad \beta_0 = \left(\frac{D}{2E} \right)^{2/3}. \quad (\text{A14})$$

The derivatives of $S(E, \beta_0)$ are given by

$$S_n = (-1)^n \frac{(2n-1)!! D}{2^n \beta_0^{(2n+1)/2}}, \quad n \geq 2, \quad (\text{A15})$$

with the expansion parameter

$$S_2 = \frac{3!!D}{2^2\beta_0^{5/2}}. \quad (\text{A16})$$

For our purposes it is more convenient to have β_0 (or $E^{-2/3}$) as the expansion parameter rather than $1/S_2$. To achieve this order by order, consider a typical term in the expansion given in Eq.(A12) of the form

$$\frac{S_{n_1}S_{n_2}\dots S_{n_k}}{S_2^m} \propto (\beta_0)^{5m/2-(2n_1+1)/2-(2n_2+1)/2-\dots-(2n_k+1)} = (\beta_0)^M. \quad (\text{A17})$$

For counting and collecting the powers in β_0 it is convenient to put $m_i = 1$ and allow repetitions of n_i . Imposing the constraints (A10) we have

$$M = \frac{5m}{2} - (n_1 + n_2 + \dots + n_k) - \frac{k}{2} = \frac{m-k}{2}, \quad n_i \geq 3, \quad (\text{A18})$$

since

$$n_1 + n_2 + \dots + n_k = 2m. \quad (\text{A19})$$

Here M is the power of β_0 in the series and k is the number of terms in the product that contribute to a given power M which may be more than one. Since $m \geq 2$ and $k \geq 1$, the lowest power is $M = 1/2$. In Tab. II we give the relevant contributions up to $M = 1/2, 1, 3/2$. The table lists all the terms which contribute at a particular order in β_0 . Putting in the numerical factors from integration as given in Eq. (A12) and collecting terms at each order, we obtain

$$\begin{aligned} g_{as}(E) = & \frac{e^{S(\beta_0)}}{\sqrt{2\pi S^{(2)}}} \left\{ 1 + \left[\frac{3!!(S_4/4!)}{(S_2)^2} - \frac{5!!(S_3/3!)^2}{2!(S_2)^3} \right] \right. \\ & + \left[-\frac{5!!(S_6/6!)}{(S_2)^3} + \frac{7!!((S_3S_5/3!5!) + (S_4/4!)^2/2!)}{(S_2)^4} - \frac{9!!(S_3/3!)^2(S_4/4!)/2!}{(S_2)^5} + \frac{11!!(S_3/3!)^4/4!}{(S_2)^6} \right] \\ & + \frac{7!!S_8}{(S_2)^4} - \frac{9!!((S_7S_3/3!7!) + (S_6S_4/6!4!) + (S_5/5!)^2/2!)}{(S_2)^5} \\ & + \frac{11!!((S_6/6!)(S_3/3!)^2/2! + (S_5S_4S_3/5!4!3!) + (S_4/4!)^3/3!)}{(S_2)^6} \\ & - \frac{13!!((S_5/5!)(S_3/3!)^3/3! + (S_4S_3/4!3!)^2/2!2!)}{(S_2)^7} \\ & + \frac{15!!((S_4/4!)(S_3/3!)^4/4!)}{(S_2)^8} \\ & \left. - \frac{17!!((S_3/3!)^6/6!)}{(S_2)^9} - \dots \right\}. \quad (\text{A20}) \end{aligned}$$

$M=(m-k)/2$	m	k	n_i	Terms
1/2	2	1	4	S_4/S_2^2
1/2	3	2	3,3	S_3^2/S_2^3
1	3	1	6	S_6/S_2^3
1	4	2	4,4	S_4^2/S_2^4
1	4	2	5,3	S_3S_5/S_2^4
1	5	3	4,3,3	$S_4S_3^2/S_2^5$
1	6	4	3,3,3,3	S_3^4/S_2^6
3/2	4	1	8	S_8/S_2^4
3/2	5	2	7,3	S_7S_3/S_2^5
3/2	5	2	6,4	S_6S_4/S_2^5
3/2	5	2	5,5	S_5^2/S_2^5
3/2	6	3	6,3,3	$S_6S_3^2/S_2^6$
3/2	6	3	5,4,3	$S_5S_4S_3/S_2^6$
3/2	6	3	4,4,4	S_4^3/S_2^6
3/2	7	4	5,3,3,3	$S_5S_3^3/S_2^7$
3/2	7	4	4,4,3,3	$S_4^2S_3^2/S_2^7$
3/2	8	5	4,3,3,3,3	$S_4S_3^4/S_2^8$
3/2	9	6	3,3,3,3,3,3	S_3^6/S_2^9

TABLE II: Contributing terms at each order in powers of β_0 . Note that $n_i \geq 3$ and hence the saturation occurs when all or most of S_n are equal to 3.

Substituting for S_n from Eq.(A15), we finally get the desired series of contributions

$$g_{as}(E) = \frac{e^{S(\beta_0)}}{\sqrt{2\pi S^{(2)}}} \left[1 - C_1 \left(\frac{\sqrt{\beta_0}}{D} \right) - C_2 \left(\frac{\sqrt{\beta_0}}{D} \right)^2 - C_3 \left(\frac{\sqrt{\beta_0}}{D} \right)^3 - \dots \right], \quad (\text{A21})$$

where

$$C_1 = \frac{5}{18} = \frac{5}{2 \times 3^2}, \quad C_2 = \frac{35}{648} = \frac{5 \times 7}{2^3 \times 3^4}, \quad C_3 = \frac{665}{34992} = \frac{5 \times 7 \times 19}{2^4 \times 3^7}. \quad (\text{A22})$$

Furthermore

$$\frac{\sqrt{\beta_0}}{D} = \left[\frac{1}{2D^2E} \right]^{1/3}, \quad D = 0.678093895. \quad (\text{A23})$$

Substituting for β_0 we finally obtain

$$g_{as}(E) = \frac{e^{S(\beta_0)}}{\sqrt{2\pi S^{(2)}}} [1 - c_1 E^{-1/3} - c_2 E^{-2/3} - c_3 E^{-1} - \dots], \quad (\text{A24})$$

with

$$c_1 = \frac{C_1}{(2D^2)^{1/3}} = 0.285645648, \quad c_2 = \frac{C_2}{(2D^2)^{2/3}} = 0.057115405, \quad (\text{A25})$$

and

$$c_3 = \frac{C_3}{(2D^2)^{3/3}} = 0.020665371. \quad (\text{A26})$$

Appendix B: Asymptotic evaluation of the Airy function

We derive here the asymptotic expressions of the real-valued Airy function $\text{Ai}(z)$, both for large positive and negative real z , using the stationary-phase method, as an illustration of the method used in the main text. In Ref. [13] this was done for integrals over the Airy function; here we do it for the Airy function itself. Its complex integral representation is given by

$$\text{Ai}(z) = \frac{1}{2\pi i} \int_C d\beta e^{S(z,\beta)}, \quad \beta = x + iy, \quad (\text{B1})$$

with

$$S(z, \beta) = -z\beta + \frac{1}{3}\beta^3. \quad (\text{B2})$$

C is a contour along the imaginary β axis, i.e. from $y = -\infty$ to $y = +\infty$, at a finite distance $x = \epsilon > 0$ (see also Fig. 1 in Ref. [13]). Let us split the function $S(z, \beta)$ in its real and imaginary part:

$$S(z, \beta) = X(x, y) + iY(x, y), \quad (\text{B3})$$

so that

$$X(x, y) = -zx + \frac{1}{3}x^3 - xy^2, \quad Y(x, y) = -zy - \frac{1}{3}y^3 + x^2y. \quad (\text{B4})$$

(We ignore the argument z which is a parameter in the real functions X and Y .) It is easy to see that the Cauchy-Riemann (CR) conditions are fulfilled for X and Y :

$$\frac{\partial X}{\partial x} = \frac{\partial Y}{\partial y} = -z + x^2 - y^2, \quad (\text{B5})$$

and

$$\frac{\partial X}{\partial y} = -\frac{\partial Y}{\partial x} = -2xy. \quad (\text{B6})$$

Therefore $S(z, \beta)$ is analytic in the whole complex β plane; it has no poles. [The shaded areas in Fig. 1 of [13] are those in which $\text{Re } \beta^3 < 0$ so that the integrand of (B1) vanishes at both ends of the contour C .]

Like in [13], we evaluate (B1) approximately in the stationary-phase approximation. To that purpose we solve the saddle-point (SP) equation and look for solutions in the complex plane.

$$\left. \frac{\partial S}{\partial \beta} \right|_{\beta_0} = -z + \beta_0^2 = 0 \quad \Rightarrow \quad \beta_0^2 = z. \quad (\text{B7})$$

For $z > 0$, we have one real solution β_0 :

$$\beta_0 = \sqrt{z} \quad \Rightarrow \quad x_0 = \sqrt{z}, \quad y_0 = 0. \quad (\text{B8})$$

(We can neglect the negative root of z for the reason given at the end of Subsect. 1 below.)

For $z < 0$, we have a pair of imaginary solutions $\beta_{1,2}$:

$$\beta_{1,2} = \pm ai \quad \Rightarrow \quad x_{1,2} = 0, \quad y_1 = a, \quad y_2 = -a, \quad a = +\sqrt{|z|}. \quad (\text{B9})$$

We now approximate the integration by the stationary-phase method, obtaining thereby the asymptotically leading contributions from the regions near the saddle points. For $z > 0$ we use the real saddle point β_0 , and for $z < 0$ the two complex-conjugate saddle points $\beta_{1,2}$. This is also shown and explained by Balasz *et al.* [13]. These authors investigated integrals over the Airy function. Our present case, the Airy function itself corresponds to taking $n = -1$ in their treatment. Although they exclude negative values of n , their results apply also for $n = -1$; the complex saddles then lie on the imaginary t axis as shown below.

1. Case $z > 0$: the exponential tail of $\text{Ai}(z)$

We first look at $z > 0$ and derive the asymptotic expression of $\text{Ai}(z)$ for $z \gg 0$, which is found from SP integration over the real saddle at $\beta_0 = x_0 = z$. We find that the curvature of $\text{Re } S = X(x_0, y)$ is negative in the y direction:

$$\left. \frac{\partial^2 X}{\partial y^2} \right|_{y_0=0} = -x_0 = -z, \quad (\text{B10})$$

(and, due to the CR conditions, positive in the x direction), so that a straight-line contour along the imaginary axis with $x_0 = z$ will lead to a maximum of $\text{Re } S$ at $y_0 = 0$. We thus

choose the contour C_0 as:

$$C_0: \quad \beta = \sqrt{z} + it, \quad t \in (-\infty, +\infty). \quad (\text{B11})$$

Expanding $S(z, \beta)$ along this contour up to order t^2 , we get

$$S_0(z, \beta) = -z(\sqrt{z} + it) + \frac{1}{3}(\sqrt{z} + it)^3 = -\frac{2}{3}z^{3/2} - \sqrt{z}t^2 + \dots, \quad (\text{B12})$$

and the integral (B1) yields the result

$$\text{Ai}(z) \sim \frac{1}{2\pi i} e^{-\frac{2}{3}z^{3/2}} \int_{-\infty}^{+\infty} idt e^{-\sqrt{z}t^2} = \frac{1}{2\sqrt{\pi}z^{1/4}} e^{-\frac{2}{3}z^{3/2}}, \quad (z \gg 0) \quad (\text{B13})$$

which is exactly the leading term of Eq. 10.4.59 in [10].

A note concerning the sign of \sqrt{z} . In principle, we have two real roots of (B7) for $z > 0$: $\beta_0 = \pm\sqrt{z}$. However, if we integrate over the saddle $x_0 = -\sqrt{z}$, $y_0 = 0$ as above, we obtain a result like (B13) but with the diverging exponential $e^{\frac{2}{3}z^{3/2}}$. This corresponds to the associated Airy function $\text{Bi}(z)$ [10] which has the same integral representation as (B1) with an appropriately chosen contour C .

2. Case $z < 0$: the oscillations of $\text{Ai}(z)$

We now want to integrate along paths that go over the imaginary saddles $\beta_{1,2}$, in order to find the asymptotic oscillations of $\text{Ai}(z)$ for $z \ll 0$. To that purpose, let us have a look at the landscape of $\text{Re} S(\beta)$ given by Eq. (B2).

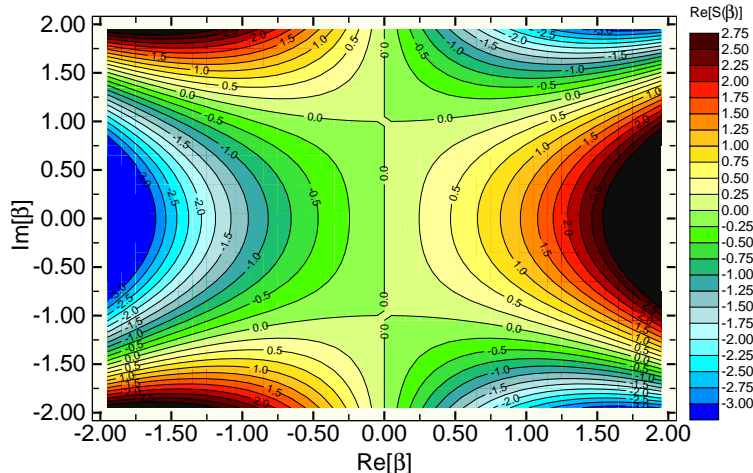


FIG. 19: Surface plot of $\text{Re} S(\beta)$ (B2) of the Airy function in the complex β plane for $z = -1$.

Figure 19 shows a plot of $\text{Re } S(\beta)$ in the complex β plane, taken for $z = -1$ (so that $a = 1$). We clearly see the two saddles at $\text{Im } \beta_{1,2} = y_{1,2} = \pm a = \pm 1$ with $\text{Re } \beta_{1,2} = 0$. We also see that $\text{Re } S$ is zero along the imaginary axis and locally (at $y_{1,2} = \pm a$) in x direction around $x_{1,2} = 0$, so that passing over the saddles in y or x direction would lead to a zero result. Instead, we have (similarly to [13]) to pass over the lower saddle (at $y_2 = -a$) from lower right to upper left (SE to NW), and over the upper saddle (at $y_1 = +a$) from lower left to upper right (SW to NE), connecting the two paths smoothly to the regions to the right of the imaginary axis where the integrand vanishes for $y \rightarrow \pm\infty$.

In order to find the directions of steepest descent (or ascent), we parameterize the contour over the saddles locally as straight lines and write them in polar coordinates (r, α)

$$x = r \cos \alpha, \quad y = r \sin \alpha. \quad (\text{B14})$$

Let us start at the upper saddle at $y_1 = +a$, $x_1 = 0$. We define a straight-line contour C_1 as:

$$C_1: \quad \beta = ia + r e^{i\alpha}, \quad r \in (-\infty, +\infty). \quad (\text{B15})$$

Along this path, the function $S(z, \beta)$ becomes (noting that $-z = a^2$)

$$S_1(z, \beta) = a^2(ia + r e^{i\alpha}) + \frac{1}{3}(ia + r e^{i\alpha})^3 = \frac{2}{3}ia^3 + iar^2 e^{2i\alpha} + \frac{1}{3}r^3 e^{3i\alpha}. \quad (\text{B16})$$

The real part of S_1 then is

$$\text{Re } S_1(r, \alpha) = X_1(r, \alpha) = -ar^2 \sin(2\alpha) + \frac{1}{3}r^3 \cos(3\alpha). \quad (\text{B17})$$

The curvature in the r direction, taken at $r = 0$, is

$$K_1(\alpha) = \left. \frac{\partial^2 X_1}{\partial r^2} \right|_{r=0} = -2a \sin(2\alpha). \quad (\text{B18})$$

This has a minimum at $\alpha = \pi/4$ and a maximum at $\alpha = 3\pi/4$. Thus the path of steepest ascent over this saddle is locally a straight line at the angle $\alpha = \pi/4$, with $K_1(\pi/4) = -2a$, so that $X_1(r, \alpha = \pi/4)$ has a maximum at $r = 0$. Along this direction the action becomes, up to order r^2 ,

$$S_1(z = -a^2, r) \simeq \frac{2}{3}ia^3 - ar^2. \quad (\text{B19})$$

Doing the integral over r (taken from $-\infty$ to $+\infty$ to complete the Gauss integral) – and not forgetting that $d\beta = e^{i\alpha} dr$ – we get the following contribution to (B1):

$$\frac{1}{2\pi i} \int_{C_1} d\beta e^{S(z, \beta)} \sim \frac{-i}{2\sqrt{\pi a}} e^{\frac{2}{3}ia^3 + i\pi/4}. \quad (\text{B20})$$

At the lower saddle ($y_2 = -a$, $x_2 = 0$), we do exactly the same, defining the contour C_2 through it:

$$C_2 : \quad \beta = -ia + r e^{i\alpha}, \quad r \in (-\infty, +\infty). \quad (\text{B21})$$

Along this path, the function $S(z, \beta)$ becomes

$$S_2(z = -a^2, r) = -\frac{2}{3}ia^3 - iar^2 e^{2i\alpha} + \frac{1}{3}r^3 e^{3i\alpha}. \quad (\text{B22})$$

Here the curvature at $r = 0$ becomes

$$K_2(\alpha) = 2a \sin(2\alpha), \quad (\text{B23})$$

which is maximum at $\alpha = \pi/4$ and minimum at $\alpha = 3\pi/4$. Thus we have to go over this saddle in the direction $\alpha = 3\pi/4$. Proceeding as above, we obtain

$$\frac{1}{2\pi i} \int_{C_2} d\beta e^{S(z, \beta)} \sim \frac{-i}{2\sqrt{\pi a}} e^{-\frac{2}{3}ia^3 + i3\pi/4}. \quad (\text{B24})$$

Adding the contributions (B20) and (B24), we obtain the following result:

$$\text{Ai}(z) \sim \frac{1}{\sqrt{\pi}|z|^{1/4}} \sin\left(\frac{2}{3}|z|^{3/2} + \pi/4\right), \quad (z \ll 0) \quad (\text{B25})$$

which is exactly the leading term of the asymptotic expression 10.4.60 in [10].

This exercise demonstrates how the use of the stationary-phase integration over complex saddles can yield asymptotic expressions for oscillating functions.